ACCSCIENCE PUBLISHING

Tumor Discovery

ORIGINAL RESEARCH ARTICLE

Innovative index for quantifying breast cancer development through T_1- and T_2-weighted magnetic resonance imaging images

Mansour Ashoor and Abdollah Khorshidi*

Radiation Applications Research School, Nuclear Science and Technology Research Institute, Atomic Energy Organization of Iran (AEOI), Tehran, Iran

Abstract

Breast cancer has recently received considerable attention in the field of diagnostic imaging. It can present in various forms, including invasive, *in situ*, or mixed subtypes. As breast tumors grow faster than other tumor types, non-invasive imaging methods, such as magnetic resonance imaging (MRI), are widely used for their quantitative assessment. This study proposes a novel function that utilizes specific mathematical relationships between relaxation times in MRI to generate maps by defining alpha star. We introduced transverse–longitudinal function (TLF), incorporating T1, T2, and alpha parameters. The function equals zero for a given assumed alpha value. Then, when plotting the TLF, a maximum amount was introduced as a percentage of the maximum width at the x-value. By calculating the inverse of the TLF, the full width at × maximum (FW×M)—the difference between the maximum and minimum alpha stars—was obtained for each image pixel. If this parameter were estimated for the entire image, only one FW×M would be obtained. The derived maps demonstrated breast tumor growth and predictive potential, with a reasonable signal-to-noise ratio of $16.5\times^{-0.096}$. While the x-value approached 1, more details in the entire breast image became visible. The resulting images with the index value of −0.096 revealed breast structures and other information at different stages, potentially facilitating the quantitative assessment of tumor characteristics and progression.

Keywords: Breast cancer; Magnetic resonance imaging; Relaxation times; Signal-to-noise ratio; Full width at x maximum

***Corresponding author:**
Abdollah Khorshidi
(abkhorshidi@yahoo.com)

Citation: Ashoor M, Khorshidi A. Innovative index for quantifying breast cancer development through T_1- and T_2-weighted magnetic resonance imaging images. *Tumor Discov*. 2026;5(1):94-105. doi: 10.36922/TD025230041

Received: June 2, 2025

Revised: September 28, 2025

Accepted: October 22, 2025

Published online: November 11, 2025

1. Introduction

Magnetic resonance imaging (MRI) is a useful tool for detecting and characterizing breast diseases, assessing the local tumor extent, evaluating treatment responses, and guiding biopsy and localization. The reported sensitivity of this procedure for detecting invasive breast cancer has been close to 100% in several studies, indicating that breast MRI is important for preoperative staging.[1] However, breast MRI has variable specificity, reported between 37% and 97%.[2] Low specificity could be a potential cause of overtreatment.[3]

Breast cancer is one of the most common malignancies in women and can present as invasive, *in situ*, or mixed tumor types. Breast cancer can be investigated using non-invasive medical imaging techniques, including breast MRI. MRI can be utilized in

combination with mammography techniques to examine high-risk cancers or better delineate suspicious regions.[4] In addition, MRI is occasionally employed as a complementary technique in breast tumor diagnosis to more accurately evaluate tumor size and detect additional or multifocal lesions.[5-10] Therefore, generating maps depicting the stages of cancer growth can aid in treatment, as discussed in this research. Specifically, diffusion-weighted imaging (DWI) can be used to detect breast malignancy.[11]

Zanotelli *et al.*[12] characterized the physical structures of the extracellular matrix during tumor progression to integrate values in the literature, identify discrepancies and similarities, and better understand how aberrant extracellular matrix dynamics contribute to cancer progression. In addition, Huang *et al.*[13] developed co-culture spheroids that regulate tumor invasion in an extracellular matrix to disclose the spatial distribution of two cell types through real-time imaging. Furthermore, Li and Thirumalai[14] used evolutionary game theory (EGT) to examine how interactions between subclone populations induce intratumoral heterogeneity.

The EGT provides a novel and unique avenue for investigating intratumoral heterogeneity, accounting for the interactions among tumor subpopulations or between cancer and normal cells.[15,16] It is a subfield of game theory, which provides mathematical models for studying the strategic interaction among individuals. An individual ("player") receives a payoff during the game depending on both the player's and the others' behavior ("strategy"). In cancer research, the players are cancer or normal cells, and the payoff is their fitness, while the strategies are phenotypes adopted by players.[17] The advantage of EGT is that it can describe the time-dependent evolution of the relative abundance of each cell type, determine the equilibrium conditions, and assess the stability of phenotypes that coexist. Such mathematical and physical simulations complement experimental research and may generate new conceptual approaches for the development of effective therapies for various cancer types.

Likewise, Rockne *et al.*[18] simulated gliomas using multiple variables and an MRI system to estimate net proliferation rates and diffusion parameters of a linear radial growth outline. Moreover, Thomas *et al.*[19] enhanced immunotherapy and targeted therapy through stromal-remodeled solid tumors and engineered bacteria. They reported a hyper-vesiculating *Escherichia coli* Nissle (ΔECHy)-based tumor-targeting bacterial system capable of delivering a fusion peptide, cytolysin A–hyaluronidase, through outer membrane vesicles. The capability of targeting hypoxic tumors, manufacturing recombinant proteins *in situ*, and the added advantage of an on-site outer membrane vesicle-based distribution system make the engineered bacterial vector a reliable candidate for peptide delivery in a live bio-therapeutic procedure.

Khalifa *et al.*[20] presented a haplotype analysis and linkage disequilibrium of breast cancer susceptibility genes (*BRCA*) in glioblastoma to identify cancer risk factors and determine the treatment response. Similarly, Wang *et al.*[21] investigated the role of pyroptosis in breast cancer patients and identified 15 prognostic genes associated with tumor growth. Furthermore, Zhang *et al.*[22] reported a case of a 38-year-old woman diagnosed with invasive ductal adenocarcinoma of the left breast in which the recurrent lesion responded to combination therapy consisting of capecitabine and pyrotinib, with tolerable adverse events. In this regard, Okwor *et al.*[23] emphasized the importance of understanding the mechanisms of modulation, tumor–immune interactions, and the potential of epigenetic therapies in improving treatment outcomes in triple-negative breast cancer (TNBC). In addition to that, Zhang *et al.*[24] examined the effects of cyclin-dependent kinase 4/6 inhibitors in breast cancer therapy to enhance immune responses. Furthermore, Aye *et al.*[25] investigated the relationship between tumor subtypes and tumor, node, or metastasis staging in breast cancer patients, in which the TNBC subtype revealed significant associations with advanced T and N stages. Also, they found no statistically significant relationship between receptor status and M stage or between human epidermal growth factor receptor 2 (HER2) status and components of tumor staging. However, Gat *et al.*[26] found that Zercepac® is effective and safe in neoadjuvant therapy for HER2-positive breast cancer.

Recently, Razem *et al.*[27] reported a case of a 50-year-old woman diagnosed with a malignant proliferating trichilemmal tumor of the scalp several years following chemotherapy for breast cancer, initially misdiagnosed as squamous cell carcinoma on biopsy. Moreover, Aref *et al.*[28] utilized optical differentiation using a hyperspectral imaging system to categorize malignant and normal tissues. Their experimental trials showed that the system could identify the optimal wavelength for diagnostic and therapeutic applications through the light interaction behavior of the breast tissue's optical properties.

During invasive therapy or mammography, ionizing radiation interacts with tissue and may expose normal tissue to energy deposition, potentially causing harm. To decrease the dose ratio while increasing efficiency and the signal-to-noise ratio (SNR), techniques based on shielding design and aspects of breast deformation were proposed.[29,30] One of these differences is the geometric and functional differences in breast structure or configuration

during imaging or treatment.[31] In contrast, MRI is a non-ionizing imaging technique and does not expose patients to ionizing radiation. The T_1- and T_2-weighted images of the abnormal breasts were considered for further analysis in this study.

This study proposes a new function that applies the corresponding MRI physics to relaxation times, generating fresh maps by defining a discrete and unique index. These derived images show the trend of breast tumor growth and tumor ratio prognosis, along with an adequate SNR.

2. Methods and materials

2.1. Principles of MRI

In nuclear magnetic resonance spectroscopy, the equilibrium state of a spin system can be perturbed by a radiofrequency (RF) magnetic field $B_1(t)$ with a frequency ω_{RF} that matches the Larmor frequency ω_0, which tilts the magnetization (M). While a nuclear magnetic moment (μ) can merely take 2I+1 discrete orientations relative to the static magnetic field B_0 (direction quantization), the M can take any direction in space and change it continuously. The effect of $B_1(t)$ rotating at ω_0 around the direction of B_0 is optimally analyzed in a rotating coordinate system, i.e., a coordinate system rotating at ω_0 around the z-axis (Figure 1). Switching to a rotating coordinate system with axes (x', y', z) has two advantages: (i) Since the x'–y' plane of the rotating system is synchronized with the RF field, the B_1 vector remains stationary in this system; and (ii) μ precesses at ω_0 around the direction of B_0. This also applies to the macroscopic sum of μ, i.e., for M.[32,33] Consequently, an observer in the rotating coordinate system will conclude that the position of M does not change. From this perspective, M behaves as if the B_0 field is absent (Larmor's theorem). In summary, the dynamics of M in the rotating coordinate system are determined solely by the static B_1 field. If this field points along the x'-axis, M precesses around the x'-axis.

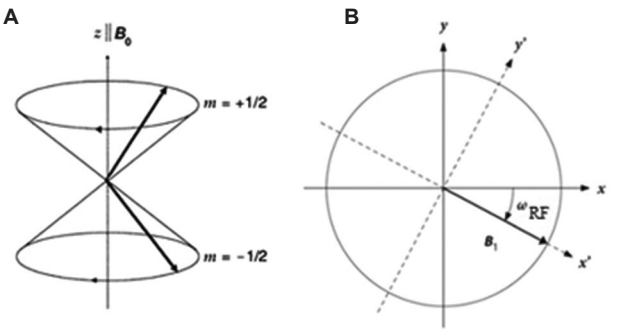

Figure 1. (A) Double precession cone for a nucleus with spin quantum number (I) of 1/2. The two allowed spin states (precession cones) are categorized by the magnetic quantum numbers (m) of ±1/2. (B) Radiofrequency (RF) field in a stationary and in a rotating coordinate system. In the stationary system (x, y, z), the magnetic field $B_1(t)$ rotates with angular frequency ω_{RF} in the x–y plane around the z-axis. If we observe this rotation from a rotating system (x', y', z) that rotates with the same angular frequency ω_{RF} around the z-axis, the vector is stationary. The rotating coordinate system is usually chosen such that the B_1 field points in the x'-direction. Figure created by the authors.

Mathematically, the relaxation times T_1 and T_2 are considered macroscopic and microscopic features, respectively. However, all types of magnetic fields are present only in the corresponding tissue within a small space. In all tissues, there are weak magnetic fields generated by spinning hydrogen nuclei. The tip of M traces a helical trajectory on the surface of a sphere around the B_0 magnetic field on the surface sphere in a helical manner, with the vector length remaining constant,[32] as shown in Figure 2.

Figure 3 shows the exponential relaxation of longitudinal and transverse magnetization moduli after the excitation of spin structure by a flip or 90° pulse and provides a rough explanation of these relaxation times. Here, T_1 specifies the time required for the longitudinal magnetization to rise to 63% of its equilibrium value M_0 after a 90° pulse, and T_2 specifies the time required for the transverse magnetization to decay to 37% of its initial value after a 90° pulse.[35]

2.2. Our proposed theory

The magnitudes of the magnetized vectors of longitudinal $M_z(t)$ and transverse $M_{xy}(t)$ are always related to each other as follows:

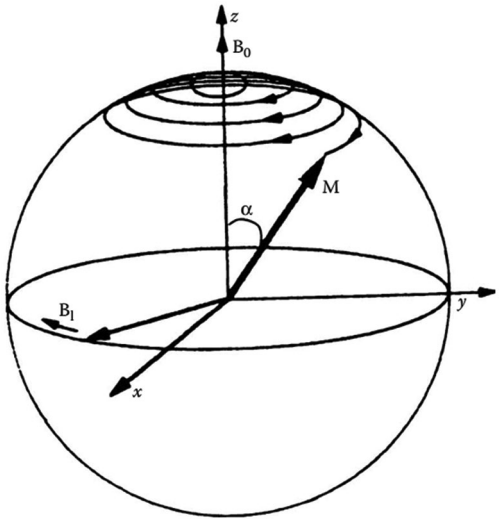

Figure 2. Schematic representation of the resonance excitation process. By rotating the reference frame at the Larmor frequency ω_0 around the path of the B_0 magnetic field, the magnetization vector M moves forward at the frequency ω_1 around the stationary B_1 magnetic field. In the stationary coordinate system, this slight rotation is overlaid by the significantly faster rotation around the z-axis. Consequently, the tip of the M vector spirals on a sphere's surface.[34] Photo published with the author's permission.

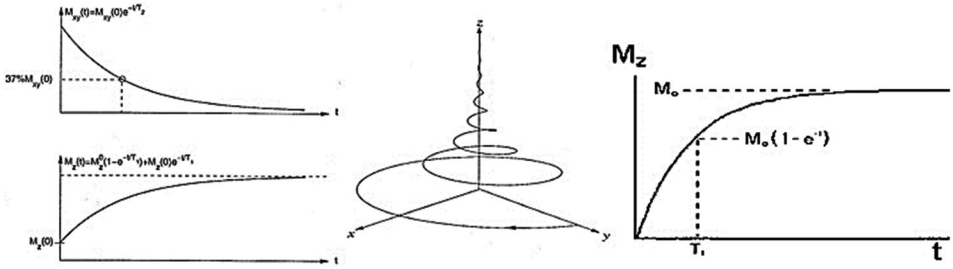

Figure 3. Relaxations of the longitudinal and transverse magnetization. The 90° pulse excitation returns the longitudinal magnetization M_z to the equilibrium value $M_z = M_0$, and successively the transverse magnetization to $M_{xy} = 0$. The *sequential progression* is indicated by the relaxation times T_1 and T_2, respectively.[36] Photo published with the author's permission.

$$\frac{T_1}{T_2} = \frac{Ln\left[\frac{M_{xy}(t)}{M_0}\right]}{Ln\left[1-\frac{M_z(t)}{M_0}\right]} \quad (1)$$

Here, the M in thermal equilibrium is described by the magnetization vector M_0, which is defined as the vector sum of the μ per unit volume. To extract and segment data from the T_1 and T_2 recordings together, a parametric function between them was proposed as follows:

$$M_z\left(\frac{T_1}{T_2}\right) = \left(\frac{T_1}{T_2}\right)^{\alpha} \times M_{xy}\left[\left(\frac{T_1}{T_2}\right)^{\alpha}\right] \quad (2)$$

where α is the parameter. After substituting the equations of $M_z(t)$ and $M_{xy}(t)$, as shown in Figure 3, into Equation (2), the parametric transverse–longitudinal function (TLF) was obtained as follows:

$$\begin{aligned} TLF &= F\left(T_1, T_2, \alpha\right) \\ &= T_1^{á} \times \exp(-T_1^{á} / T_2^{á+1}) + T_2^{á} \times \exp(-1/T_2) - T_2^{á} \end{aligned} \quad (3)$$

Using the TLF (α) function, the absolute values of the α* were calculated from the following function:

$$\alpha^* = TLF^{-1}\{x \times [\max(TLF(\alpha))]\} \quad (4)$$

Where x is a parameter ranging from 0 to 1. Finally, a new index was designed as full width at × maximum (FW×M) to generate new maps with an appropriate SNR:

$$FW \times M = \alpha^*_{max} - \alpha^*_{min} \quad (5)$$

The defined new index was calculated using the Matlab software (R2016a, MathWorks Inc., United States) and evaluated using different relaxation times and various values of the proposed x-parameter to obtain the new maps, the so-called FW×M map.

3. Results

The combination of spin–spin and spin–lattice relaxation times under proper conditions can characterize breast cancer. The T_1- and T_2-weighted images of the abnormal breast from the study by Han *et al.*,[37] indicated as number 86 (# 86), were chosen for simulation and generation of FW×M maps at different indices (x = 0.01, 0.03, 0.09, 0.1, 0.11, 0.2, 0.3, 0.4, 0.5, 0.6, 0.7, 0.8, 0.9 and 1), as shown in Figure 4.

At lower x-parameter values, tumor details were better displayed on the FW×M maps. As the x-parameter increased, all breast elements were displayed. Therefore, the FW×M maps can forecast the growth trend of breast cancer at different x-parameters.

The evaluation of breast tumors at any stage is crucial for diagnosis and for considering both treatment planning and the prediction of tumor growth rate. The prediction and quantitative assessment were performed by defining a theory and corresponding recommendations in MRI, creating FW×M maps with an appropriate SNR. These maps can improve breast cancer diagnosis. The main symptom of breast cancer is a new mass or nodule, for which positron-emitting radionuclides can be utilized for breast cancer treatment. However, the geometric configuration of this mass must first be estimated. The dynamic maps resulting from the proposed theory can help to depict these configurations precisely. Imaging can aid in identifying suspicious lesions, monitoring tumor extent, and assessing treatment response.

4. Discussion

Breast cancer remains a leading cause of cancer mortality among women worldwide. The heterogeneity of breast cancer, manifested in varying growth rates, angiogenic profiles, and metastatic potentials, necessitates individualized treatment strategies. Dynamic contrast-

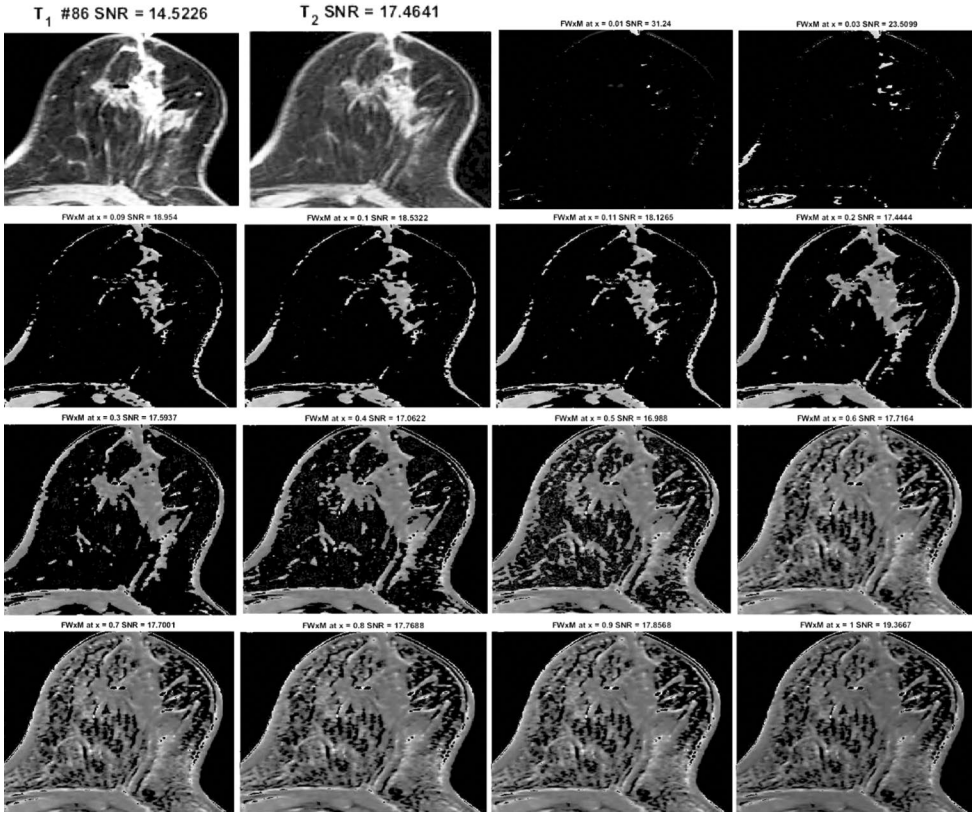

Figure 4. The FW×M maps were obtained from T_1- and T_2-weighted images of the abnormal breast from the study by Han *et al.*[37] at various x-parameters—x = 0.01, 0.03, 0.09, 0.1, 0.11, 0.2, 0.3, 0.4, 0.5, 0.6, 0.7, 0.8, 0.9, and 1. As the x-value increases toward 1, the details of healthy and tumorous areas become more visible simultaneously.

enhanced MRI (DCE-MRI) has emerged as a gold-standard imaging modality for breast cancer detection, staging, and response assessment. It provides not only high-resolution morphological data but also functional information by tracking the uptake and washout of a gadolinium-based contrast agent, which is indicative of tissue vascularity, perfusion, and permeability. Current clinical practices rely on empirical metrics from DCE-MRI, such as the signal enhancement ratio or qualitative descriptors from the Breast Imaging Reporting and Data System (BI-RADS).[38-41] While useful, these metrics are descriptive rather than predictive. They offer a snapshot in time but lack a formal mathematical framework to forecast future tumor states.

The core scientific problem is to transition from description to prediction. A mathematical function that can reliably predict growth would allow clinicians to:

(i) Estimate time-to-critical size
(ii) Simulate response to different neoadjuvant therapies in silico
(iii) Identify aggressive phenotypes based on their predicted kinetic parameters
(iv) Optimize the timing of surgical intervention.

Mei *et al.*[42] examined the DCE-MRI method based on fuzzy C-mean clustering in the analysis of invasive breast carcinoma and reported favorable diagnostic performance. The limitation of their research is that they compared the clustering effects of two algorithms. On the other hand, hormones play a role in cancers; however, the exact origin is unclear. Breast tumors usually arise from the cells of the milk ducts and, sometimes, from the lobules; occasionally, they originate in other tissues. In most cases, breast cancer arises from epithelial cells within the breast ducts or lobules. It is often a type of carcinoma called adenocarcinoma. This carcinoma arises from the glandular tissue. Other forms may also occur in the breast tissue, such as sarcomas, which form in muscle cells, fat cells, and connective tissues. In some cases, a single breast tumor can encompass different classes or a group of *in situ* and invasive cancers. These cancers can be divided into several groups depending on the proteins in the breast cancer cells, for example, triple-negative or hormone-receptor-positive cancers. Ductal carcinoma *in situ* often manifests as pre-invasive or non-invasive cancer cells.[43-46] The new maps derived from our research can help explore these groups for better diagnosis.

A tumor can be viewed as a tissue in which neoplastic cells are embedded in a specific micro-environment that modulates tumor cell behavior during multistep tumorigenesis. Given this, antineoplastic therapy should be tailored to target not only tumor cells but also the cellular components of the tumor micro-environment (TME). This requirement becomes clear when considering tumor angiogenesis, a significant aspect of cancer biology. Ion channels and transporters are increasingly acknowledged as relevant players in tumor cell–TME interactions. For example, in tumor neoangiogenesis, soluble elements, as well as solid components of the extracellular matrix and membrane proteins, determine the signaling exchange between the TME and the involved cell types. The signaling network is organized by functional nodes, which may consist of integrin receptors that associate with other proteins to create macromolecular signaling platforms at the adhesion sites. These complexes often contain ion channels. Recently, Crociani *et al.*[47] proposed a simple mathematical model for adhesion-mediated signaling in cancer to model novel signaling pathways of ether-à-go-go–related gene channels (*HERG1*) and integrins via a tumor suppressor gene to control angiogenesis. Using mathematical models, they demonstrated that a dynamic switch between conditions of normoxia and cell death occurs without considering the interconnected dynamics of the key microscopic players.

Since the physical characteristics of the extracellular matrix strongly influence malignancy and tumor progression, Engelke[48] established a close connection between tumor biology and extracellular matrix to address tumor signaling directly and indirectly through the modulation of tumor interactions. Moreover, Margarit *et al.*[49] proposed a spherical model for cellular automation in a solid tumor with plasticity to study the spread of cancer cells to other organs. However, they only considered the mean diameters of solid tumors, for example, 0.2 cm in breast cancer, without considering tumor heterogeneity in recurrence or metastasis.

Cabuk *et al.*[50] differentiated benign and malignant breast lesions of cysts and intramammary lymph nodes using the DWI technique and calculated apparent diffusion coefficient (ADC) values of both lesions. Meanwhile, Oohashi *et al.*[51] reviewed the usefulness of ADC values for characterizing benign and malignant tumors through DWI. Advanced DWI models are usually challenged by long acquisition times, prompting research into simplified approaches. One method involves estimating intravoxel incoherent motion (IVIM) and non-Gaussian parameters using just a few b-values. Chan *et al.*[52] presented a method for breast tumor characterization by combining IVIM and DWI techniques through 13 b-values to identify tumor heterogeneity and differentiate low- and high-cellularity regions. Kurt *et al.*[53] examined the usefulness of diffusion tensor imaging (DTI) and DWI in assessing axillary lymph nodes (ALNs) of breast cancer patients and evaluated morphological features, ADC, volume anisotropy, and fractional anisotropy values. They indicated that the ADC value of metastatic ALNs is meaningfully lower than that of non-metastatic ALNs, and DTI metrics of metastatic ALNs are considerably higher than those of non-metastatic ALNs. In their investigation, ADC had a better diagnostic performance than morphological features, fractional anisotropy, and volume anisotropy. Mao *et al.*[54] explored the value of quantitative parameters derived from diffusion spectrum imaging (DSI) in preoperatively predicting HER2 status in patients with breast cancer. They concluded that DSI could be helpful for preoperative prediction of HER2, but DSI alone may not be sufficient in predicting HER2 status preoperatively in patients with breast cancer.

The evaluation of cell differentiation and its consequences is currently providing new groundwork for theoretical and experimental research. Clinical data regularly show that various elements are responsible for tumor growth, spread, metastasis, and recurrence, particularly after therapy. In this study, the characterization of regional tumor differentiation was investigated utilizing experimental data from a previous study,[37] and a proposed theory, based on T1- and T2-weighted MRI images of the abnormal breast, was examined to assess SNR performance and visualize tumor-related changes.[55,56]

Nowadays, breast cancer can be diagnosed using MRI. Early detection of high-risk breast cancer is crucial for the adaptation of appropriate and effective interventional therapies. If the tumor is detected at an early stage, it can be treated rapidly.[57,58] The novel maps attained in this study can depict the stages of breast cancer growth locally, as well as the estimated size of the mass. The goal of mammography is to detect cancer cells before they cause symptoms. Breast tumors are often detected when they tend to grow abnormally, potentially indicating spread from the breast. In contrast, the model proposed in this study can regularly detect tumors at an early stage, when they remain confined to the breast tissue. The common use of mammography has increased the detection of breast tumors before the onset of clinical symptoms. Nevertheless, mammography does not always differentiate between various types of breast tumors, either because specific studies have not been conducted or because certain breast tumors remain radiographically occult even under optimal imaging conditions.[59-61] In this context, combining T_1 and T_2 relaxation times, as demonstrated in the proposed framework, may provide

approaches for characterizing breast cancer. The obtained FW×M maps at various indices, with proper SNR, may enable visualization of early tumor spread. At lower values of the x-parameter, the details of breast structures adjacent to abnormal areas were better visualized on the FW×M maps, whereas higher x-parameter values rendered all breast elements visible.

Lu *et al.*[62] compared breast density measurements of fatty and fibroglandular tissues using MRI and digital mammography and demonstrated that the correlation was stronger between the two MRI methods than between MRI and mammography. Furthermore, Jarrett *et al.*[63] presented a calibration-based protocol that predicts breast cancer, and a quantitative perfusion and diffusion model to generate spatially resolved predictions of individual tumor response to therapy. In addition, Patel *et al.*[64] developed a biological mathematical model to predict the response of patients with locally advanced breast cancer to neoadjuvant therapy, describing the spatiotemporal changes in tumor cell numbers using a logistic regression model based on predicted tumor volume metrics. As anisotropic diffusion is typically assessed with DTI—a method that applies diffusion gradients in several spatial directions—Ortiz-Abellán *et al.*[65] proposed a classification model to distinguish healthy from tumor-affected pixels and to evaluate isotropic tissues such as the breast. For isotropic diffusion, the mathematical modeling of diffusion signal evolution is generally based on exponential decay functions. The most commonly used model is the mono-exponential model, which introduces ADC to represent the total effect of both slow and fast displacements. However, this model does not differentiate among the underlying diffusion mechanisms. To address this problem, the IVIM, a pseudo-biexponential model, has been proposed to separate slow diffusion from fast diffusion. Although the IVIM model is theoretically more physiologically relevant, the mono-exponential model is still the most broadly used due to its simplicity.

Davenport *et al.*[66] developed a coupled ordinary differential equation model of TNBC with compartments that represent tumor proliferation, necrosis, apoptosis, and immune response to computationally describe the biological effects of combined chemotherapy with doxorubicin and paclitaxel. Their model was parameterized using longitudinal ^{18}F-fluorothymidine positron emission tomography (PET) imaging data, allowing for a non-invasive molecular imaging approach to quantify tumor proliferation and volume in two murine TNBC models. In general, a robust mathematical model should describe both tumor volume changes and the extent of necrosis to provide insight into the optimal ordering, dosing, and timing of doxorubicin and paclitaxel treatment. Campana *et al.*[67] reported the use of radiomics in MRI images for pre-treatment molecular characterization of breast tumors, thereby improving existing predictive models. Dedicated breast PET systems can achieve higher spatial resolution compared with whole-body PET and enable tumor delineation comparable to MRI, while also providing metabolic information that often precedes the vascular and morphological changes induced by treatment. The integration of these imaging-derived factors is accomplished through multiparametric imaging.

In the present study, the TLF was introduced as a combination of three parameters: T_1, T_2, and α, which can be zero for a specific value of α (Equation [3]). When the TLF function becomes zero, α reaches its maximum value, and the corresponding line coincides with the horizontal axis. Plotting the TLF function yields a maximum amplitude, which we expressed as a percentage of the maximum width at a given x-value. By taking the inverse of the TLF function, an interval called FW×M was determined. This parameter represents the difference between the maximum and minimum α^* values (Equation [5]). As the x-value changes, both the maximum and minimum α^* values vary, resulting in a specific FW×M parameter for each image pixel. Calculating this parameter across all pixels yields a composite FW×M value for the entire image. Subsequently, SNR was calculated to assess structural visibility across the breast. As the x-value increased toward 1, as shown in Figure 4, the details of healthy areas and tumor regions became more clearly visualized. In general, higher x-values improved the visualization of overall breast structures. The corresponding SNR values as a function of x (ranging from 0 to 1) are shown in Figure 5. Because FW×M represents the difference between the minimum and maximum α^* values, SNR calculation facilitated clearer detail recognition across the image, particularly at higher x-values ($SNR = 16.5\times^{-0.096}$). As shown in Figure 5, various regression functions were fitted to the acquired graph, and the optimal equation was identified as:

$$y=ax^{-b} \quad (6)$$

This innovative index (b) of −0.096 enables the visualization of breast structures and finer details at various stages, supporting the quantitative assessment of potential breast cancer indicators. Overall, the SNR values decreased from 31.24 to 19.37 as × increased from 0.01 to 1, with minor fluctuations observed between the × indices of 0.11 and 0.90, corresponding to a slight linear slope of 0.14.

Since artificial intelligence (AI)-based imaging algorithms can predict invasive breast cancers, the integration of AI into cancer detection and prediction has

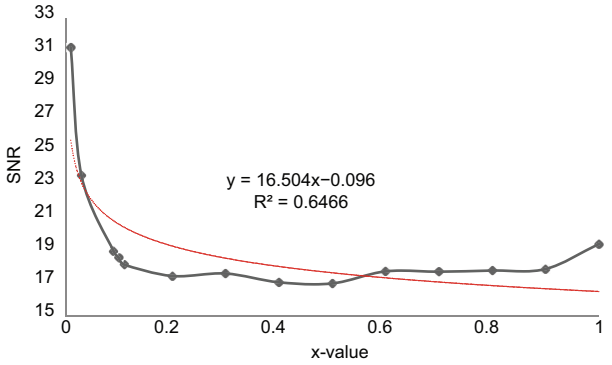

Figure 5. The achieved signal-to-noise ratio (SNR) values with respect to the x intervals between 0 and 1. Since FW×M represents the difference between the minimum and maximum α*, increasing x-values led to improved structural detail across the entire breast image, following the relationship SNR=16.5×−0.096.

the potential to revolutionize oncology and improve patient care.[68,69] The use of various machine learning algorithms, such as deep learning,[70] has become common practice for assessing tumor grade and improving the accuracy of breast cancer prediction. In addition, combining advanced diagnostic and treatment strategies can shorten the patient evaluation period.[71-76]

Clinically, a painless, firm mass with uneven edges is often suggestive of malignancy, particularly when located in deeper levels, and may become tender or rupture over time. Other characteristic features of breast tumors include swelling, skin dimpling or irritation, breast tissue or nipple pain, redness, scaling, skin or nipple induration, and nipple discharge or retraction.[77-80] Anatomically, the mammary glands consist of a vast chain of lobular ducts lined with epithelium that secrete milk, which drains through larger milk-bearing ducts converging at the nipple. These glandular structures are embedded within supporting fatty tissue, and the breasts are divided into lobules by connective tissue. The maps obtained in this study were able to depict these anatomical structures and surrounding tissues at various stages with finer details.

5. Conclusion

The accurate prediction of breast cancer growth dynamics is a critical component of personalized oncology, influencing treatment planning, timing of interventions, and prognostic assessment. While DCE-MRI provides exceptional soft-tissue contrast and captures physiological parameters related to tumor angiogenesis, current clinical evaluations are predominantly qualitative or semi-quantitative. This study proposed the definition and theoretical foundation for a new mathematical function, the TLF, designed to quantitatively model and predict tumor growth by integrating key biomechanical and physiological parameters derived from T_1- and T_2-weighted images. This function, along with its corresponding index, enables the estimation of tumor-related signal changes across different stages, thereby supporting more informed treatment planning. The outcomes revealed that the generated maps demonstrated adequate SNR. Overall, the development of such a predictive function holds significant potential for advancing precision medicine in breast cancer care.

Acknowledgments

None.

Funding

None.

Conflict of interest

The authors declare that they have no competing interests.

Author contributions

Conceptualization: All authors
Data curation: All authors
Formal analysis: All authors
Investigation: All authors
Methodology: All authors
Software: All authors
Supervision: Abdollah Khorshidi
Validation: All authors
Visualization: Abdollah Khorshidi
Writing–original draft: All authors
Writing–review & editing: All authors

Ethics approval and consent to participate

Not applicable.

Consent for publication

Not applicable.

Availability of data

All data required to support the results and conclusions of the study have been included in this manuscript.

References

1. Orel SG, Schnall MD. MR imaging of the breast for the detection, diagnosis, and staging of breast cancer. *Radiology.* 2001;220(1):13-30.

   doi: 10.1148/radiology.220.1.r01jl3113

2. Esserman L, Wolverton D, Hylton N. Magnetic resonance imaging for primary breast cancer management: Current role and new applications. *Endocr Relat Cancer.* 2002;9:141-153.

doi: 10.1677/erc.0.0090141

3. Van Goethem M, Schelfout K, Dijckmans L, *et al*. MR mammography in the pre-operative staging of breast cancer in patients with dense breast tissue: Comparison with mammography and ultrasound. *Eur Radiol.* 2004;14(5): 809-816.

   doi: 10.1007/s00330-003-2146-7

4. Roganovic D, Djilas D, Vujnovic S, Pavic D, Stojanov D. Breast MRI, digital mammography and breast tomosynthesis: Comparison of three methods for early detection of breast cancer. *Bosn J Basic Med Sci.* 2015;15(4):64-68.

   doi: 10.17305/bjbms.2015.616

5. Shahbazi-Gahrouei D, Aminolroayaei F, Nematollahi H, Ghaderian M, Gahrouei SS. Advanced magnetic resonance imaging modalities for breast cancer diagnosis: An overview of recent findings and perspectives. *Diagnostics.* 2022;12(11):2741.

   doi: 10.3390/diagnostics12112741

6. Ashoor M, Khorshidi A. Improving signal-to-noise ratio by maximal convolution of longitudinal and transverse magnetization components in MRI: Application to the breast cancer detection. *Med Biol Eng Comput*. 2024;62(3):941-954.

   doi: 10.1007/s11517-023-02994-w

7. Daimiel Naranjo I, Lo Gullo R, Saccarelli C, *et al*. Diagnostic value of diffusion-weighted imaging with synthetic b-values in breast tumors: Comparison with dynamic contrast-enhanced and multiparametric MRI. *Eur Radiol.* 2021;31:356-367.

   doi: 10.1007/s00330-020-07094-z

8. Alshorman J, Karaminasian M, Sadeghi S, Safari E, Abbaspourtabari H, Altahla R. Prevalence of somatic symptom disorder in Syrian patients with breast cancer: A cross-sectional study. *J Clin Basic Psychosom.* 2025:025150023.

   doi: 10.36922/JCBP025150023

9. Malik S, Malik A, Islam J, *et al*. Breaking the metabolic code in triple-negative breast cancer: Mechanistic insights into glycolytic enzyme inhibitors for suppressing metastasis and tumor growth. *Cancer Plus.* 2025;7(2):25-45.

   doi: 10.36922/cp.8363

10. Khorshidi A, Shams-Abadi M. Simulation of 52m + gMn production yield via chromium target under low-energy proton irradiation from mashhad small cyclotron. *Phys Part Nuclei Lett.* 2025;22:586-595.

    doi: 10.1134/S1547477125700219

11. Ashoor M, Khorshidi A. Estimation of the number of compartments associated with the apparent diffusion coefficient in MRI: The theoretical and experimental investigations. *Am J Roentgenol.* 2016;206(3):455-462.

    doi: 10.2214/AJR.15.14497

12. Zanotelli MR, Chada NC, Johnson CA, Reinhart-King CA. The physical microenvironment of tumors: Characterization and clinical impact. *Biophys Rev Lett.* 2020;15(2):51-82.

    doi: 10.1142/S1793048020300029

13. Huang YL, Shiau C, Wu C, Segall JE, Wu M. The architecture of co-culture spheroids regulates tumor invasion within a 3D extracellular matrix. *Biophys Rev Lett.* 2020;15(3):131-141.

    doi: 10.1142/S1793048020500034

14. Li X, Thirumalai D. Cooperation among tumor cell subpopulations leads to intratumor heterogeneity. *Biophys Rev Lett.* 2020;15(2):99-119.

    doi: 10.1142/S1793048020300042

15. Dingli D, Chalub FA, Santos FC, Van Segbroeck S, Pacheco JM. Cancer phenotype as the outcome of an evolutionary game between normal and malignant cells. *Br J Cancer.* 2009;101(7):1130-1136.

    doi: 10.1038/sj.bjc.6605288

16. Li X, Thirumalai D. Share, but unequally: A plausible mechanism for emergence and maintenance of intratumour heterogeneity. *J R Soc Interface*. 2019;16(150):20180820.

    doi: 10.1098/rsif.2018.0820

17. Archetti M, Pienta KJ. Cooperation among cancer cells: Applying game theory to cancer. *Nat Rev Cancer*. 2019;19:110-117.

    doi: 10.1038/s41568-018-0083-7

18. Rockne R, Alvord JREC, Reed PJ, Swanson KR. Modeling the growth and invasion of gliomas, from simple to complex: The goldie locks paradigm. *Biophys Rev Lett.* 2008;3(1-2):111-123.

    doi: 10.1142/S1793048008000642

19. Thomas SC, Madaan T, Kamble NS, Siddiqui NA, Pauletti GM, Kotagiri N. Engineered bacteria enhance immunotherapy and targeted therapy through stromal remodeling of tumors. *Adv Healthc Mater.* 2022;11(2):e2101487.

    doi: 10.1002/adhm.202101487

20. Khalifa MK, Nageeb AM, Mohamed MM, Ezz El Arab LR, Swellam M. Haplotype analysis and linkage disequilibrium of BRCA genes in glioblastoma: Impact on treatment response. *Tumor Discov.* 2024;3(1):1480.

    doi: 10.36922/td.1480

21. Wang S, Yang D, Mo J, Chen M, Zhang R. The role of pyroptosis-related genes in breast cancer progression. *Tumor Discov.* 2024;3(3):3469.

    doi: 10.36922/td.3469

22. Zhang Y, Chen B, Wu J, Chen C. Efficacy of pyrotinib and capecitabine in recurrent breast cancer with a HER2-negative genetic switch following systemic therapy: A case report and

literature review. *Tumor Discov.* 2025;4(1):113-119.

doi: 10.36922/td.4093

23. Okwor VC, Okwor CJ, Musayayi SA, *et al*. Immune modulation and epigenetic therapies for enhanced outcome of treatment in triple-negative breast cancer. *Tumor Discov.* 2024;3(3):3383.

doi: 10.36922/td.3383

24. Zhang Y, Chen B, Lin S, Zhang R, Wu J, Chen C. Emerging immunomodulatory effects of CDK4/6 inhibitors in breast cancer therapy: A comprehensive review. *Tumor Discov.* 2025;4(3):025190037.

doi: 10.36922/TD025190037

25. Aye SM, Zu WWM. Characterizing breast cancer in Myanmar: Insights from receptor status and tumor staging. *Tumor Discov.* 2025:025250051.

doi: 10.36922/TD025250051

26. Gao H, Lei J, Gui Z, Wang S. Comparative efficacy and safety of Zercepac® plus pyrotinib versus Zercepac® plus pertuzumab in combination with chemotherapy as neoadjuvant therapy for HER2-positive breast cancer: A retrospective study. *Eurasian J Med Oncol.* 2025;9:025100044.

doi: 10.36922/EJMO025100044

27. Razem B, Ilhami O, Hamid SE, Oukerroum A, Slimani F. Malignant proliferating trichilemmal tumor post-chemotherapy: A case report. *Tumor Discov.* 2024;3(2):2344.

doi: 10.36922/td.2344

28. Aref MH, Aboughaleb IH, Hussein AA, Farag AM, El-Ghaffar SA, El-Sharkawy YH. Malignant versus normal breast tissue: Optical differentiation exploiting hyperspectral imaging system. *Tumor Discov.* 2023;2(1):258.

doi: 10.36922/td.258

29. Sosu EK. *Optimization of Radiological Protection of Patients Undergoing Mammography Examination in Ghana. PhD Dissertion*. University of Cape Coast; 2018. Available from: http://ir.ucc.edu.gh/jspui/handle/123456789/3432 [Last accessed on 2022 May 12].

30. Poma GE. *Development and Tomographic Reconstruction of an Innovative MBI Device for the Early Breast Cancer Diagnosis. PhD Dissertion, Università Degli Studi di Catania*; 2020. Available from: https://hdl.handle.net/20.500.14242/75383 [Last accessed on 2020 Jul 07].

31. Khorshidi A, Ashoor M, Abdollahi A. Optimization of breast treatment planning towards lower dose rate: A Monte Carlo simulation study. *Inform Med Unlocked.* 2023;38:101220.

doi: 10.1016/j.imu.2023.101220

32. Brix G, Kolem H, Nitz WR, *et al*. Basics of magnetic resonance imaging and magnetic resonance spectroscopy. In: Reiser M, Semmler W, Hricak H, editors. *Magnetic Resonance Tomography*. Berlin, Heidelberg: Springer; 2008.

doi: 10.1007/978-3-540-29355-2_2

33. Abele M. *Solid-State NMR Spectroscopy for Structural Investigations in Materials Science. PhD Dissertion*. Institute of Physical Chemistry, University of Stuttgart, Stuttgart; 2012. Available from: https://www.ipc.uni-stuttgart.de/roduner/phd-theses [Last accessed on 2008 Jan 01].

34. Landini L, Positano V, Santarelli MF, editors. *Advanced Image Processing in Magnetic Resonance Imaging*. London: CRC Press; 2018.

35. Bloch F, Hansen WW, Packard M. The nuclear induction experiment. *Phys Rev.* 1946;70:474.

doi: 10.1103/PhysRev.70.474

36. Liang ZP, Lauterbur PC. *Principles of Magnetic Resonance Imaging: A Signal Processing Perspective.* Washington, DC: The Institute of Electrical and Electronics Engineers Press; 2000.

37. Han SH, An YY, Kang BJ, Kim SH, Lee EJ. Takeaways from pre-contrast T1 and T2 breast magnetic resonance imaging in women with recently diagnosed breast cancer. *Iran J Radiol.* 2016;13(4):e36271.

doi: 10.5812/iranjradiol.36271

38. Byrne H. Dissecting cancer through mathematics: from the cell to the animal model. *Nat Rev Cancer.* 2010;10:221-230.

doi: 10.1038/nrc2808

39. AlBuainain RY, Bunajem FY, Abdulla HA. Assessment of tumor response to neoadjuvant chemotherapy in breast cancer using MRI and 18F-FDG PET/CT. *Eur J Breast Health.* 2025;21(1):46-51.

doi: 10.4274/ejbh.galenos.2024.2024-8-2

40. Qadir A, Singh N, Moe AAK, *et al*. Potential of MRI in assessing treatment response after neoadjuvant radiation therapy treatment in breast cancer patients: A scoping review. *Clin Breast Cancer.* 2025;25(1):e1-e9.e2.

doi: 10.1016/j.clbc.2024.05.010

41. Lorenzon M, Zuiani C, Londero V, Linda A, Furlan A, Bazzocchi M. Assessment of breast cancer response to neoadjuvant chemotherapy: Is volumetric MRI a reliable tool? *Eur J Radiol.* 2009;71(1):82-88.

doi: 10.1016/j.ejrad.2008.03.021

42. Mei L, Wang K, Gu Y. Improved fuzzy C-means clustering algorithm-based dynamic contrast-enhanced magnetic resonance imaging features in the diagnosis of invasive breast carcinoma before and after menopause. *Comput Math Methods Med.* 2022;2022(1):2917844.

doi: 10.1155/2022/2917844

43. Kang J, Jiang N, Shataer M, Tuersong T. Quantitative bibliometric insights into cisplatin resistance in breast cancer (2010–2024): Implications for drug development. *Cancer Plus.* 2025;7:025220037.

doi: 10.36922/CP025220037

44. Greenberg S, Rugo HS. Triple-negative breast cancer: Role of antiangiogenic agents. *Cancer J.* 2010;16(1):33-38.

doi: 10.1097/PPO.0b013e3181d38514

45. Steinhauer V, Sergeev NI. Radiomics: Phases of osteoclastic metastasis status in breast cancer identified by morphologic markers. *Cancer Plus.* 2025;7(1):109-115.

doi: 10.36922/cp.6649

46. Stewart DA, Winnike JH, McRitchie SL, Clark RF, Pathmasiri WW, Sumner SJ. Metabolomics analysis of hormone-responsive and triple-negative breast cancer cell responses to paclitaxel identify key metabolic differences. *J Proteome Res.* 2016;15(9):3225-3240.

doi: 10.1021/acs.jproteome.6b00430

47. Crociani O, Becchetti A, Fanelli D, Arcangeli A. Adhesion-mediated signalling in cancer: Recent advances and mathematical modelling. *Biophys Rev Lett.* 2014;9(3):285-300.

doi: 10.1142/S1793048014300047

48. Engelke H. Physics of the extracellular matrix and biology of tumors - a close relationship. *Biophys Rev Lett.* 2020;15(3):121-130.

doi: 10.1142/S1793048020300030

49. Margarit DH, Romanelli L, Fendrik AJ. A 3D cellular automaton for cell differentiation in a solid tumor with plasticity. *Biophys Rev Lett.* 2018;13(1):19-28.

doi: 10.1142/S1793048018500029

50. Cabuk G, Duce MN, Özgür A, Apaydin FD, Polat A, Orekici G. The diagnostic value of diffusion-weighted imaging and the apparent diffusion coefficient values in the differentiation of benign and malignant breast lesions. *J Med Imaging Radiat Oncol.* 2015;59(2):141-148.

doi: 10.1111/1754-9485.12273

51. Oohashi M, Mizuhashi F, Sugawara Y, Saegusa H, Ogura I. Diffusion-weighted magnetic resonance imaging in the palatal tumors: Usefulness of apparent diffusion coefficient value for characterization of benign and malignant tumors. *Oral Sci Int.* 2020;17(3):142-146.

doi: 10.1002/osi2.1058

52. Chan SW, Lin CA, Ouyang YC, *et al.* Characterizing breast tumor heterogeneity through IVIM-DWI parameters and signal decay analysis. *Diagnostics (Basel).* 2025;15(12):1499.

doi: 10.3390/diagnostics15121499

53. Kurt N, Kurt BB, Gulsaran U, *et al.* Diffusion tensor imaging and diffusion-weighted imaging on axillary lymph node status in breast cancer patients. *Diagn Interv Radiol.* 2022;28(4):329-336.

doi: 10.5152/dir.2022.21460

54. Mao C, Jiang W, Huang J, *et al.* Quantitative parameters of diffusion spectrum imaging: HER2 status prediction in patients with breast cancer. *Front Oncol.* 2022;12:817070.

doi: 10.3389/fonc.2022.817070

55. Ashoor M, Khorshidi A, Pirouzi A, Abdollahi A, Mohsenzadeh M, Barzi SMZ. Estimation of Reynolds number on microvasculature capillary bed using diffusion and perfusion MRI: The theoretical and experimental investigations. *Eur Phys J Plus.* 2021;136:152.

doi: 10.1140/epjp/s13360-021-01145-0

56. Ashoor M, Khorshidi A, Sarkhosh L. Estimation of microvascular capillary physical parameters using MRI assuming a pseudo liquid drop as model of fluid exchange on the cellular level. *Rep Pract Oncol Radiother.* 2019;24(1):3-11.

doi: 10.1016/j.rpor.2018.09.007

57. López MT, Feltri AP, Isabe GF, Guida V, Fernandes A, Blanch R. Risk and protective factors associated with breast cancer. *Cancer Plus.* 2020;2(3):1-6.

doi: 10.18063/cp.v2i3.351

58. Elbiad O, Mazour O, Ennibi K, Badaoui B, Laraqui A. Variants of unknown significance in BRCA1 and BRCA2 among breast cancer patients in Middle Eastern and North African populations: A systematic review. *Eurasian J Med Oncol.* 2025;9(1):16-45.

doi: 10.36922/ejmo.5800

59. Monzon AZ, Franco-López Á, Culebras JM. Benefits and harms of screening: Overdiagnosis and anticipatory medicine – A secondary publication. *Tumor Discov.* 2022;1(2):228.

doi: 10.36922/td.v1i2.228

60. Humayun S, Mahmood T. Artificial intelligence for early diagnosis of breast cancer in women: A systematic literature review. *Artif Intell Health.* 2025;2(2):100-116.

doi: 10.36922/aih.4197

61. Colman RD, Kotera Y. Addressing the psychological impact of infertility risk arising from breast cancer treatment: Education and self-compassion interventions. *Int J Popul Stud* 2025;11(5):31-37.

doi: 10.36922/ijps.1724

62. Lu LJW, Nishino TK, Johnson RF, *et al.* Comparison of breast tissue measurements using magnetic resonance imaging, digital mammography and a mathematical algorithm. *Phys Med Biol.* 2012;57:6903.

doi: 10.1088/0031-9155/57/21/6903

63. Jarrett AM, Kazerouni AS, Wu C, *et al.* Quantitative magnetic resonance imaging and tumor forecasting of breast cancer patients in the community setting. *Nat Protoc.* 2021;16:5309-5338.

doi: 10.1038/s41596-021-00617-y

64. Patel RJS, Wu C, Stowers CE, *et al*. MRI-based mathematical modeling to predict the response of I-SPY 2 breast cancer patients to neoadjuvant therapy. *Clin Cancer Res.* 2025.

doi: 10.1158/1078-0432.CCR-25-0668

65. Ortiz-Abellán C, Aguado-Sarrió E, Prats-Montalbán JM, Camps-Herrero J, Ferrer A. New breast cancer biomarkers from diffusion magnetic resonance imaging based on the Diffusion Tensor using multivariate curve resolution (MCR) models. *Chemometr Intell Lab Syst.* 2024;251:105171.

doi: 10.1016/j.chemolab.2024.105171

66. Davenport AA, Lu Y, Gallegos CA, *et al*. Mathematical model of triple-negative breast cancer in response to combination chemotherapies. *Bull Math Biol.* 2023;85:7.

doi: 10.1007/s11538-022-01108-1

67. Campana A, Gandomkar Z, Giannotti N, Reed W. The use of radiomics in magnetic resonance imaging for the pre-treatment characterisation of breast cancers: A scoping review. *J Med Radiat Sci.* 2023;70(4):462-478.

doi: 10.1002/jmrs.709

68. Nafiss N, Heiranizadeh N, Shirinzadeh-Dastgiri A, *et al*. The application of artificial intelligence in breast cancer. *Eurasian J Med Oncol.* 2024;8(3):235-244.

doi: 10.14744/ejmo.2024.45903

69. Haider S. Catalyzing breast cancer diagnosis: Ai advancements in mammography. *Eurasian J Med Oncol.* 2023;7(4):402-403.

doi: 10.14744/ejmo.2023.93033

70. Botlagunta M, Botlagunta M, Venkata MD, Kanakapudi C, Khan Z. Correlation-based comparative machine learning analysis for the classification of metastatic breast cancer using blood profile. *Eurasian J Med Oncol.* 2024;8(2):152-164.

doi: 10.14744/ejmo.2024.52521

71. Bandyopadhyay A, Mondal HS, Dam B, Patranabis DC, Pal B. Innovative infrared imaging approach for breast cancer screening: Integrating rotational thermography and machine learning analysis. *Artif Intell Health.* 2024;1(3):64-79.

doi: 10.36922/aih.3312

72. Leong HJY, Tan HD, Yap WH, Chia AYY, Zacchigna S, Tang YQ. Identification of potentially therapeutic target genes in metastatic breast cancer via integrative network analysis. *Eurasian J Med Oncol.* 2023;7(4):371-387.

doi: 10.14744/ejmo.2023.80452

73. Ashoor M, Khorshidi A. Extraction of hybrid data using intrinsic interactions of relaxation times in MRI. *Int J Biomath.* 2025.

doi: 10.1142/S1793524525500159

74. Liu X, Hong Z, Ding H, *et al*. Assessment of cerebral venous sinus: Anatomical and functional diagnostic performance of three-dimensional reconstruction models based on venous sinus MRI and CT images. *Brain Heart.* 2024;2(2):2756.

doi: 10.36922/bh.2756

75. Ashoor M, Khorshidi A. Introducing a parametric function on relaxation times in magnetic resonance imaging. *Multimed Tools Appl.* 2025;84:18247-18262.

doi: 10.1007/s11042-024-19789-2

76. Khorshidi A. Examining neural correlates of sexual preferences between Persian homo- and heterosexual males using psychological assessments and functional magnetic resonance imaging in specifying cognitive map: A limited and cross-sectional study. *J Pediatr Neurol.* 2024;21:1-16.

doi: 10.1055/s-0044-1788630

77. Khorshidi A, Ashoor M. New deformity outline on the breast radiation therapy for diminishing absorbed dose ratio. *Braz J Radiat Sci.* 2023;11(3):1-12.

doi: 10.15392/2319-0612.2023.2281

78. Jensen JR, Do D, Chang YP, *et al*. CoreView imaging on needle: Rapid core-needle biopsy imaging for point-of-care breast cancer diagnosis. *Global Transl Med.* 2025;4:025170039.

doi: 10.36922/GTM025170039

79. Khorshidi A. Segmentation of tumor region in respiratory disease by extended algorithm. *Int J Mod Phys C.* 2023;34(12):2350164.

doi: 10.1142/S0129183123501644

80. Puvvula PK, Puvvula RS. Clinical advancements in breast cancer research: A comprehensive review. *Tumor Discov.* 2025:025090016.

doi: 10.36922/TD025090016